2024 IEEE Intelligent Vehicles Symposium (IV)
June 2-5, 2024. Jeju Island, Korea

Negotiation in Cooperative Maneuvering using Conflict Analysis: Theory and Experimental Evaluation

Hao M. Wang, Sergei S. Avedisov, Onur Altintas, and Gábor Orosz

***Abstract*— Negotiation is a class of cooperation enabled by vehicle-to-everything (V2X) communication, which involves the exchange of maneuver requests and responses between road users. In this paper, we develop criteria for request initiation and response generation under a unified conflict analysis framework. This leads to guaranteed maneuver feasibility in request and response that satisfy user-based behavior preferences. We implement negotiation via commercially available V2X devices, and experimentally evaluate the benefits of negotiation in conflict resolution. We demonstrate that negotiation can significantly benefit time efficiency of maneuvers while ensuring safety, compared to lower levels of cooperation such as status-sharing and intent-sharing. These benefits and their degradation under communication delays are quantified.**

I. Introduction

Vehicle-to-everything (V2X) communication opened up new solutions to improve traffic safety and efficiency by enabling cooperative maneuvers between vehicles [1]. Such cooperation may be centralized or decentralized [2]. Centralized cooperation relies on a traffic coordinator prescribing maneuvers for road users, while a decentralized one offers vehicles the advantage to decide on their own actions. Decentralized cooperation may be categorized into three classes: status sharing, intent sharing, and negotiation [3]. In status sharing, connected vehicles gain situational awareness by sharing their instantaneous states (e.g., position and speed). A standardized example is the basic safety message (BSM) [4]. In intent sharing, vehicles anticipate future traffic behavior by sharing motion plans, e.g., trajectories [5] or kinematic variable bounds [6]. However, status and intent sharing only allow for passive decision making. That is, a vehicle cannot cancel an unfavorable intended maneuver of a neighboring vehicle. Also, uncertainties in status and intent can lead to inefficient decisions. Instead, negotiation, as a higher-class cooperation, allows vehicles to reach agreements about their future maneuvers by actively requesting road space and responding to such requests. This leads to unambiguous conflict resolution prior to maneuver initiation.

Standardization of negotiation is in progress. For example, the society of automotive engineers (SAE) is standardizing maneuver sharing and coordination service [7], while the European Telecommunications Standards Institute (ETSI) is establishing maneuver coordination service [8]. The ongoing standardization has triggered increasing research activities. For instance, maneuver coordination was studied in [9] and [10] based on the planned and desired trajectories. In [11] an experimental proof-of-concept was provided for negotiation using automated vehicles. From a communication viewpoint, [12] performed simulations to evaluate different negotiation patterns. Most existing negotiation frameworks, however, ignore maneuver feasibility in initiating requests, by neglecting other vehicles' behavior preferences. The corresponding design criteria for feasible request timings and responses are missing. Moreover, to our best knowledge, the benefits of negotiation compared to lower-level cooperation have never been experimentally evaluated. The effects of delays in the negotiation protocol on the maneuver performance also have not been investigated. This paper bridges these gaps.

In this study, we develop mathematically rigorous criteria for request initiation and response generation under a unified framework, which enables feasible and personalized negotiation. To do so, we utilize the conflict analysis tool proposed in our previous work [13]. Such tool interprets status and intent information for fast decision making and reliable control design in conflict resolution. We then implement negotiation using commercially available V2X communication devices, and experimentally evaluate the benefits of negotiation via real vehicle-based experiments at a test track. Compared to sharing status and intent information only [6], experimental data demonstrate that negotiation can eliminate uncertainty in decision making, improving time efficiency and traffic throughput. However, these benefits diminish as the communication delay associated with negotiation increases. We quantify the benefits of negotiation and their degradation with time delay, under different vehicle operating speeds.

II. Modeling Vehicle Dynamics and Communication

As an application for negotiation, we consider the unsignalized intersection scenario depicted in Fig. 1(a). Here, the vehicle 2 (blue) seeks to perform a right turn onto the main road as the vehicle 1 (white) approaches. Nevertheless, our framework below applies to a general class of maneuvers such as left turns, merges, and roundabouts. Both vehicles are assumed to be automated and capable of V2X communication. Without V2X connectivity both vehicles would suffer from limited line of sight due to obstacles, e.g., a truck parked at the roadside. A conflict zone is defined in the intersection as highlighted by red shading. A conflict occurs when both vehicles appear in the conflict zone (even

Hao M. Wang and Gábor Orosz are with the Department of Mechanical Engineering, University of Michigan, Ann Arbor, MI 48109, USA. {haowangm, orosz}@umich.edu.

Sergei S. Avedisov and Onur Altintas are with Toyota Motor North America R&D – InfoTech Labs, Mountain View, CA 94043, USA. {sergei.avedisov, onur.altintas}@toyota.com.

Gábor Orosz is also with the Department of Civil and Environmental Engineering, University of Michigan, Ann Arbor, MI 48109, USA.

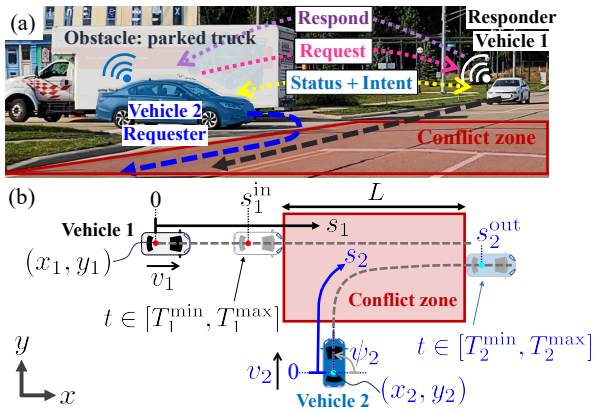

Fig. 1. Experimental setup for validating negotiation in cooperative maneuvering. (a) An unsignalized intersection scenario involving connected vehicles 1 and 2. (b) Generalized model.

partially) at the same time.

Fig. 1(b) shows a generalized model. In the Earth-fixed frame (x, y), vehicle i is localized using its rear axle center point (x_i, y_i) and yaw angle ψ_i, $i = 1, 2$. We assume that each vehicle has a planned path to follow, generated by its motion planner. We express the path using the traveled distance s_i of rear axle center point, i.e., $[x_i(s_i), y_i(s_i), \psi_i(s_i)]$. This is often referred to as arclength parameterization. Here without loss of generality, we set $s_i = 0$ at the initial time, defined as the moment when the vehicles establish communication. The path is given such that for any $[x_i, y_i, \psi_i]$ along the path, one can uniquely identify the corresponding s_i. For instance, the arclength of vehicle i entering and exiting the conflict zone can be calculated as s_i^{in} and s_i^{out}, respectively, once given the path and the geometry of conflict zone; see s_1^{in} and s_2^{out} in Fig. 1(b). A mathematically rigorous description is given in Section IV-A using clothoids.

For simplicity of analysis, we model the vehicles' longitudinal dynamics along the given path using the arclength coordinate s_i, while ignoring rolling resistance and air drag:

$$\dot{s}_i(t) = v_i(t), \qquad \dot{v}_i(t) = u_i(t), \qquad i = 1, 2. \tag{1}$$

Here the dot represents time derivative, v_i denotes the longitudinal velocity of vehicle i along its path, and u_i is used for the corresponding control input (acceleration). Both vehicles' behaviors are subject to physical limits:

$$v_i(t) \in [v_{\min,i}, v_{\max,i}], \quad u_i(t) \in [a_{\min,i}, a_{\max,i}], \quad \forall t. \tag{2}$$

We define the system state as $\mathbf{x} := [s_1\ v_1\ s_2\ v_2]^\top \in \Omega$, with $\Omega := [0, s_1^{\text{out}}] \times [v_{\min,1}, v_{\max,1}] \times [0, s_2^{\text{out}}] \times [v_{\min,2}, v_{\max,2}]$.

Using V2X communication, the two vehicles may negotiate about their conflict-free passing order, on top of the two lower-level classes of communication: status sharing and intent sharing. In status sharing, vehicles periodically share their most recent motion information, i.e., s_i and v_i. In intent sharing the information about the vehicles' future behaviors is shared. A formal definition of a vehicle's longitudinal motion intent in this intersection scenario is given below.

Definition 1: Given the dynamics (1)-(2), the longitudinal motion intent of vehicle i is represented by a restricted velocity domain $v_i(t) \in [\underline{v}_i(t), \overline{v}_i(t)]$ and acceleration (input) domain $u_i(t) \in [\underline{a}_i(t), \overline{a}_i(t)]$ over the time period $t \in [\hat{t}, \hat{t} + T]$, along a planned path $[x_i(s_i), y_i(s_i), \psi_i(s_i)]$ for $s_i \in [s_i(\hat{t}), s_i(\hat{t}) + S]$. Here $\hat{t}$ is the time when this intent is generated, T is the intent time horizon, S is the path length, and $v_{\min,1} \le \underline{v}_1(t) \le \overline{v}_1(t) \le v_{\max,1}$, $a_{\min,1} \le \underline{a}_1(t) \le \overline{a}_1(t) \le a_{\max,1}$. ■

An example of right-turn intent shared by a real vehicle in our experiments is visualized in Fig. 4. As detailed in Section IV-A, the planned path can be parameterized as a function of arclength s_i, while the intended velocity and acceleration bounds can be parameterized as functions of time t. Definition 1 thus enables compact communication implementation and is applicable to most traffic maneuvers. The intent of an automated vehicle may be generated by its motion planner, encoding specific behavior preferences. A receiver of such intent can numerically integrate the dynamics (1)-(2) using the sender's intent bounds along its path, to achieve continuous-time prediction. The intent horizon T and the path length S shall be designed long enough for informative conflict prediction, i.e., until the vehicles clear the conflict zone. Accordingly, the intent bounds shall not allow a vehicle to stop indefinitely before passing the conflict zone. For simplicity, we consider that status and intent are shared in a synchronized manner such that both vehicles have access to each other's latest status and intent at discrete times t_k, $k = 0, 1, \ldots$. For non-synchronous status and intent sharing, one may refer to our previous work [6].

While status sharing enables situational awareness and intent sharing provides anticipation into future environments, the vehicles' passing order is still implicit and the resultant passive decision-making can be conservative. For example, the uncertainty encoded in vehicle 1's intent may inhibit a timely conflict-free turning of vehicle 2. This in turn would cause unnecessary waiting and low traffic efficiency. Instead, negotiation is able to eliminate ambiguity by allowing a vehicle to explicitly transmit a maneuver request; see Fig. 1(a). The receiver(s) of this request may then respond by accepting, rejecting, or providing maneuver suggestions to the requester via V2X.

III. Negotiation using Conflict Analysis

In this section, we construct a framework for negotiation in cooperative maneuvering, which provides criteria to determine (i) a proper request initiation timing; (ii) a proper response. To do so, we utilize the conflict analysis tool developed in our previous work [13]. Noting that the requester is usually the one without right-of-way, we consider vehicle 2 as the requester and vehicle 1 as the responder. Our analysis below assumes negligible communication and computation delays, while the potential effects of time delay will be evaluated using experimental data in Section IV-B.

We are interested in whether the vehicle 2, without right-of-way, can pass the conflict zone before the vehicle 1 enters. This is formally described by the proposition

$$P := \{\exists t, (s_2(t) = s_2^{\text{out}}) \wedge (s_1(t) \le s_1^{\text{in}})\}, \tag{3}$$

where $\wedge$ is the conjunction "and", while s_1^{in} and s_2^{out} are determined from the vehicles' intended paths; see Fig. 1(b).

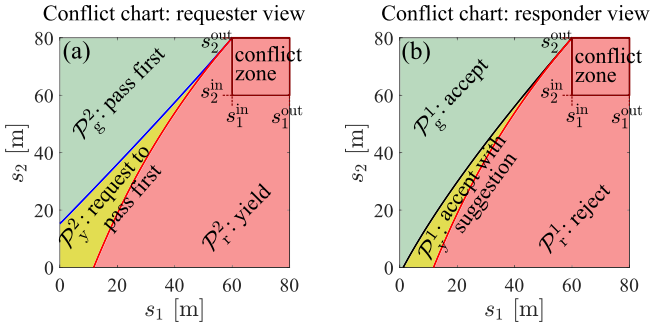

Fig. 2. An example of conflict charts in the (s_1, s_2) plane for $(v_1, v_2) = (13, 15)$ [m/s], from the perspectives of (a) vehicle 2 (requester); and (b) vehicle 1 (responder). Here, we use constant intent bounds for illustrative purposes: $\underline{v}_1(t) = \underline{v}_2(t) \equiv 5$ [m/s], $\overline{v}_1(t) = \overline{v}_2(t) \equiv 18$ [m/s], $\underline{a}_1(t) \equiv -1.2$ [m/s^2], $\overline{a}_1(t) \equiv 1.2$ [m/s^2], $\underline{a}_2(t) \equiv -0.8$ [m/s^2], and $\overline{a}_2(t) \equiv 0.8$ [m/s^2], with $s_1^{\text{in}} = s_2^{\text{in}} = 60$ [m], $s_1^{\text{out}} = s_2^{\text{out}} = 80$ [m].

From the perspective of vehicle 2, the proposition P can be decomposed into three cases:

(i) No-conflict case: Independent of the motion of vehicle 1, vehicle 2 is able to *pass first* without conflict.
(ii) Uncertain case: Depending on the motion of vehicle 1, vehicle 2 may be able to *pass first* without conflict.
(iii) Conflict case: Independent of the motion of vehicle 1, vehicle 2 is not able to *pass first* without conflict.

The three cases above correspond to the following three pairwise disjoint sets in the state space Ω of the system (1):

$$\mathcal{P}^2_{\text{g}} := \{\mathbf{x} \in \Omega | \forall u_1(t), \exists u_2(t), P\}, \tag{4}$$
$$\mathcal{P}^2_{\text{y}} := \{\mathbf{x} \in \Omega | (\exists u_1(t), \forall u_2(t), \neg P) \wedge (\exists u_1(t), \exists u_2(t), P)\}, \tag{5}$$
$$\mathcal{P}^2_{\text{r}} := \{\mathbf{x} \in \Omega | \forall u_1(t), \forall u_2(t), \neg P\}, \tag{6}$$

where $\neg$ means negation and the subscripts "g", "y", and "r" correspond to green, yellow, and red colors in visualizing the no-conflict, uncertain, and conflict sets. The superscript "2" highlights that the state space is partitioned from vehicle 2's perspective. Note that $\mathcal{P}^2_{\text{g}} \cup \mathcal{P}^2_{\text{y}} \cup \mathcal{P}^2_{\text{r}} = \Omega$. Fig. 2(a) illustrates an example of these sets in the (s_1, s_2) plane for the indicated velocities v_1, v_2, and vehicle intents. We refer to such chart as conflict chart, whose derivation is discussed further below.

At a status/intent receiving time t_k, by locating the system state $\mathbf{x}$ on the conflict chart, vehicle 2 is able to reason about conflict in terms of passing first. If $\mathbf{x}(t_k) \in \mathcal{P}^2_{\text{g}}$, then negotiating with vehicle 1 is not necessary since vehicle 2 may confidently pass first without a conflict. If $\mathbf{x}(t_k) \in \mathcal{P}^2_{\text{r}}$, then vehicle 2 is unable to pass first without a conflict under vehicle 1's intent, and shall yield without negotiation. Note that a vehicle's intent represents the benefit that it aims to secure, and thus, violating such intent is considered non-negotiable. For $\mathbf{x}(t_k) \in \mathcal{P}^2_{\text{y}}$, a conflict may occur when vehicle 2 passes first, depending on the future behavior of vehicle 1. Then, vehicle 2 may initiate a pass-first request via V2X to the vehicle 1. Feasibility of such request is justified by the predicate $(\exists u_1(t), \exists u_2(t), P)$ in the definition (5) of $\mathcal{P}^2_{\text{y}}$. Fig. 2(a) summarizes this request initiation mechanism on the conflict chart. Note that without negotiation, vehicle 2 would make a conservative decision to yield in the $\mathcal{P}^2_{\text{y}}$ region due to the uncertainty in vehicle 1's behavior [13].

Once receiving the vehicle 2's request to pass first, the vehicle 1 shall respond based on whether it can cooperate to pass second without a conflict. That is, vehicle 1 shall examine proposition P from its own perspective. By swapping u_1 and u_2 in each predicate of (4)-(6), one obtains the no-conflict, uncertain, and conflict sets partitioning the state space Ω from the vehicle 1's perspective:

$$\mathcal{P}^1_{\text{g}} := \{\mathbf{x} \in \Omega | \forall u_2(t), \exists u_1(t), P\}, \tag{7}$$
$$\mathcal{P}^1_{\text{y}} := \{\mathbf{x} \in \Omega | (\exists u_2(t), \forall u_1(t), \neg P) \wedge (\exists u_2(t), \exists u_1(t), P)\}, \tag{8}$$
$$\mathcal{P}^1_{\text{r}} := \{\mathbf{x} \in \Omega | \forall u_2(t), \forall u_1(t), \neg P\}, \tag{9}$$

where $\mathcal{P}^1_{\text{g}} \cup \mathcal{P}^1_{\text{y}} \cup \mathcal{P}^1_{\text{r}} = \Omega$ and these sets are still pairwise disjoint; see Fig. 2(b) for the corresponding conflict chart under the same parameters used for Fig. 2(a).

If the system state $\mathbf{x}(t_k) \in \mathcal{P}^1_{\text{r}}$, the request shall be rejected since a conflict-free maneuver is impossible. Note, however, that the definitions (6) and (9) indicate $\mathcal{P}^2_{\text{r}} = \mathcal{P}^1_{\text{r}}$, i.e., both vehicles have the same awareness of danger under status and intent sharing. Thus, if vehicle 2 initiates request based on conflict analysis, such request would not lead to $\mathbf{x}(t_k) \in \mathcal{P}^1_{\text{r}}$. On the other hand, similar equality does not hold for the no-conflict and uncertain sets; cf. Fig. 2(a)-(b). In fact, definitions (5), (7), (8) yield $\mathcal{P}^2_{\text{y}} \subseteq \mathcal{P}^1_{\text{g}} \cup \mathcal{P}^1_{\text{y}}$, i.e., when receiving a conflict analysis-based request, vehicle 1 may either see $\mathbf{x}(t_k) \in \mathcal{P}^1_{\text{g}}$ or $\mathcal{P}^1_{\text{y}}$. For $\mathbf{x}(t_k) \in \mathcal{P}^1_{\text{g}}$, vehicle 1 may simply accept the request. For $\mathbf{x}(t_k) \in \mathcal{P}^1_{\text{y}}$, conflict is uncertain depending on the requester's future behavior. However, the predicate $(\exists u_2(t), \exists u_1(t), P)$ in the definition (8) of $\mathcal{P}^1_{\text{y}}$ guarantees the existence of a feasible maneuver realization that satisfies both vehicles' intent while fulfilling the request. Thus, the vehicle 1 may accept the request while prescribing a conflict-free maneuver suggestion to the requester. Note that the feasibility of such suggestion indicates its acceptability to the requester, and therefore, negotiation may be finished in one round. Such response generation rule is summarized in Fig. 2(b).

Before discussing the design of maneuver suggestion, we introduce the following Theorem, which provides a criterion on checking the system state $\mathbf{x}$ using critical time parameters.

Theorem 1: Given the dynamics (1)-(2), the current state $\mathbf{x}(t_k)$, and both vehicles' intent in Definition 1, we have

$$\mathbf{x}(t_k) \in \mathcal{P}^2_{\text{g}} \iff T_1^{\min} \geq T_2^{\min}, \tag{10}$$
$$\mathbf{x}(t_k) \in \mathcal{P}^2_{\text{y}} \iff T_1^{\min} < T_2^{\min} \leq T_1^{\max}, \tag{11}$$
$$\mathbf{x}(t_k) \in \mathcal{P}^2_{\text{r}} \iff \mathbf{x}(t_k) \in \mathcal{P}^1_{\text{r}} \iff T_2^{\min} > T_1^{\max}, \tag{12}$$
$$\mathbf{x}(t_k) \in \mathcal{P}^1_{\text{g}} \iff T_1^{\max} \geq T_2^{\max}, \tag{13}$$
$$\mathbf{x}(t_k) \in \mathcal{P}^1_{\text{y}} \iff T_2^{\min} \leq T_1^{\max} < T_2^{\max}, \tag{14}$$

Here, $T_2^{\min}$ and $T_2^{\max}$ are the times t such that $s_2(t) = s_2^{\text{out}}$ under $u_2(t) \equiv \overline{a}_2(t)$ and $u_2(t) \equiv \underline{a}_2(t)$, $t \geq t_k$, respectively. $T_1^{\min}$ and $T_1^{\max}$ are the times t such that $s_1(t) = s_1^{\text{in}}$ under $u_1(t) \equiv \overline{a}_1(t)$ and $u_1(t) \equiv \underline{a}_1(t)$, $t \geq t_k$, respectively.

Proof: See Appendix I. ∎

As illustrated in Fig. 1(b), $T_2^{\min}$ and $T_2^{\max}$ are the estimated minimum and maximum times of the vehicle 2 exiting the conflict zone given its current status and intent. Similarly,

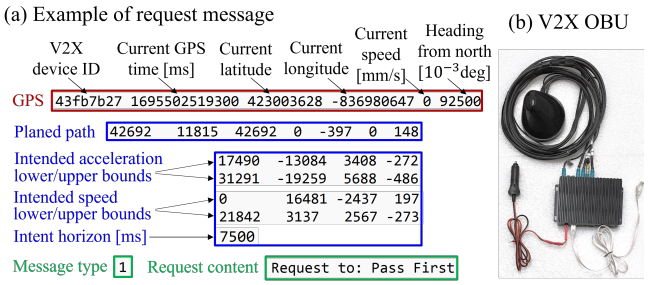

Fig. 3. Creating negotiation messages. (a) An example of a request message implemented using V2X protocol WSMP. (b) V2X on-board unit.

$T_1^{\min}$ and $T_1^{\max}$ represent the estimated minimum and maximum times of the vehicle 1 entering the conflict zone under its intent. Using these time parameters, Theorem 1 provides an efficient algorithm to determine proper request initiation timing and response based on the location of $\mathbf{x}$ in state space.

For the case $\mathbf{x}(t_k) \in \mathcal{P}_{\mathrm{y}}^1$, Theorem 1 provides a guidance on designing conflict-free maneuver suggestions in the response. From (14), if the requesting vehicle 2 decreases $T_2^{\max}$ by increasing its intended input lower bound such that

$$T_2^{\max} \in [T_2^{\min}, T_1^{\max}], \tag{15}$$

then $\mathbf{x}(t_k) \in \mathcal{P}_{\mathrm{g}}^1$ holds based on (13). That is, by imposing $T_1^{\max}$ as the requester's time deadline to clear the conflict zone, its pass-first request can be fulfilled without a conflict. Thus, (15) constitutes a valid maneuver suggestion to vehicle 2. Note that the time deadline $T_1^{\max}$ represents the negotiation limit of the responder in terms of time efficiency, and is feasible for the requester considering its given intent. We emphasize that such suggestion aims to reduce the uncertainty in the requester's intent, eliminating potentially adversarial behaviors in conducting the requested maneuver. While other types of suggestions (e.g., a specific control input) may also be considered, the proposed time deadline suggestion is efficient in computation and communication, and provides freedom on the requester's control execution.

The constructed negotiation framework is experimentally demonstrated in the next section using real vehicles.

IV. Experiments

In this section, we first create wireless messages needed for negotiation, and then present experimental results.

A. Creating Negotiation Messages

To enable efficient communication in negotiation, we implement messages of intent-sharing, request, and response under a unified design format, which encodes the vehicle's (i) current GPS information; (ii) motion intent; (iii) message type; and (iv) request/response content. Note that such design can fit into the current SAE standardization of the maneuver sharing and coordinating service [3]. Fig. 3(a) shows an example of a request message transmitted in our experiment.

Here, the vehicle's intent consists of two parts: the planned path and the intended velocity/acceleration bounds; cf. Definition 1. The planned path in Fig. 3(a) is compactly represented by seven parameters. As visualized in Fig. 4(a) and

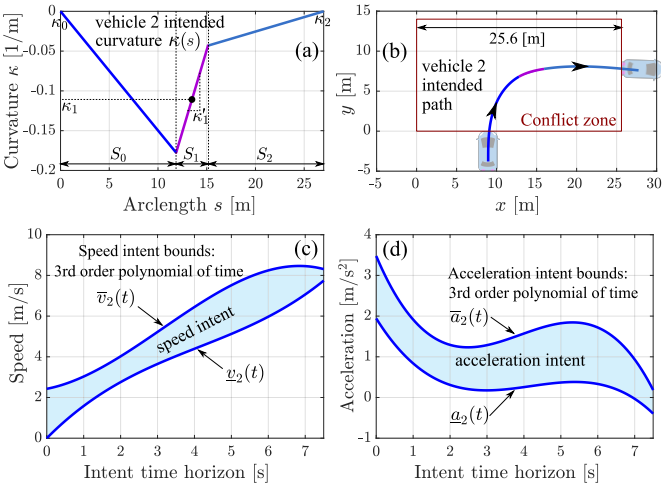

Fig. 4. Right-turn intent of vehicle 2 in the experiments. (a) Intended curvature along arclength, where the indicated $(S_0, S_1, S_2, \kappa_0, \kappa_1, \kappa_2, \kappa_1')$ correspond to the (scaled) path parameters in Fig. 3(a). Here, S_0, S_1, and S_2 are the lengths of three path segments, κ_0 and κ_2 are the initial and end curvatures, κ_1 is the curvature at the middle point of the second segment, and κ_1' is the corresponding sharpness. (b) Three-clothoid path on (x, y) plane corresponding to (a). (c)-(d) Intended speed and acceleration.

explained in its caption, these parameters specify the path's curvature κ as a three-segment piecewise linear function along its arclength s. Such curvature function $\kappa(s)$, together with the vehicle's current GPS position and heading, determine the intended path as three consecutive clothoids; see the corresponding path in the (x, y) plane in Fig. 4(b). Without loss of generality, we set the origin at the bottom-left corner of the rectangular conflict zone used in our experiment. The mathematical details of converting $\kappa(s)$ to a path in the (x, y) plane can be found in [5]. The bounds of velocity and acceleration are represented using third order polynomials of time, that is, each bound is given by four parameters; see Fig. 3(a) and its visualization in Fig. 4(c)-(d). All intent parameters in Fig. 3(a) are obtained by data fitting using right-turn maneuver data of a real vehicle with a particular driver, and are scaled to integers for compact encoding.

In accordance with the SAE standardization [3], we indicate the message type by integers: 0–intent sharing, 1–request, and 2–response. As shown in Fig. 3(a), the content of request/response is explicitly included in the message for interpretability during the experiments. Thanks to the compact implementation, our negotiation message is lightweight, with a size around 100 Bytes. The messages are implemented on commercially available V2X onboard units (OBUs) shown in Fig. 3(b), using WAVE Short Message Protocol (WSMP) [14], which allows custom messages to be transmitted at a user-determined rate. The transmission of negotiation messages is implemented in C code through the application programming interface (API) of our OBU supplier.

B. Experimental Evaluation of Negotiation

Having implemented negotiation messages, we test negotiation for conflict resolution using real vehicles at the Mcity test track of the University of Michigan. Fig. 1(a) illustrates the experimental setup, where the blue vehicle 2 intends to take a right turn (from standstill) to the main road,

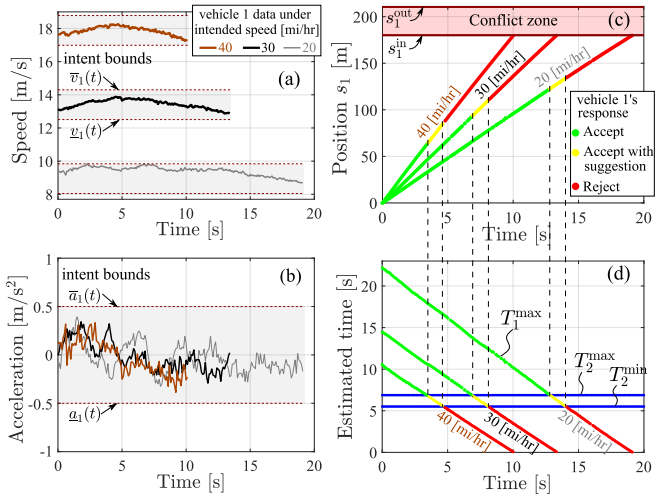

Fig. 5. Experiments of negotiation in the intersection scenario of Fig. 1 using real vehicles. (a)-(c) The responding vehicle 1's speed, acceleration, and position profiles under different approaching target speeds. The responses generated during the experiments are indicated by color in panel (c). (d) The corresponding conflict analysis showing the evolution of estimated times $T_1^{\max}$, $T_2^{\min}$, and $T_2^{\max}$.

while the white vehicle 1 is approaching on the main road. We also tested the left-turn negotiation in the experiments, but this paper only presents right-turn negotiation results due to qualitative similarity and space limits. The length of the conflict zone is $L = 25.6$ [m] according to the size of the intersection. Both vehicles are human-driven and equipped with V2X OBUs. Indeed, to fully utilize the developed negotiation framework, the vehicles shall possess high enough automation levels to execute the post-negotiation maneuvers. Our experiments, however, focus on testing the conflict analysis-based negotiation protocol and evaluating the benefits of negotiation. Thus, it is sufficient to test with connected human-driven vehicles.

The turning vehicle 2 sends its request (see Fig. 4 for its maneuver intent) and vehicle 1 responds to the request as it approaches with different pre-designed behaviors on the main road. Such setup allows us to validate a personalized response that distinguishes between different behavior preferences of vehicle 1. Fig. 5(a)-(b) show speed and acceleration data corresponding to three different approaching behaviors of vehicle 1 with target speeds 20 [mi/hr] (≈ 8.9 [m/s]), 30 [mi/hr] (≈ 13.4 [m/s]), and 40 [mi/hr] (≈ 17.9 [m/s]) and intended speed deviation within ± 2 [mi/hr] (≈ 0.9 [m/s]) from the target speeds; see gray shadings in Fig. 5(a). The intended acceleration is within $[-0.5, 0.5]$ [m/s^2] for all target speeds. Note that the profiles in Fig. 5(a)-(b) are plotted until the vehicle 1 entered the conflict zone, and the initial time is the moment when the vehicle 1 was 180 [m] away from the conflict zone.

The requesting vehicle 2 broadcasts its pass-first request periodically at 10 [Hz] (without conflict analysis) while being stationary in front of the conflict zone; see Fig. 3(a) for the message example. Such simplified request initiation allows us to thoroughly test the response part of negotiation. The responding vehicle 1 uses an onboard computer to implement the conflict analysis algorithm in Theorem 1 via C program while approaching along the main road. Conflict analysis is triggered upon the reception of a request message, which contains the latest status and intent of the requester. The corresponding response is then transmitted by the responder.

Fig. 5(c) plots the responding vehicle 1's position profile (arclength s_1) under three different approaching speeds. The data points are plotted at each request receiving time and colored according to the generated response. The corresponding conflict analysis is visualized in Fig. 5(d) through the estimated times $T_1^{\max}$, $T_2^{\min}$, and $T_2^{\max}$ (cf. Theorem 1), which are calculated onboard in real-time during the experiments. When the responder is far away, $\mathbf{x} \in \mathcal{P}_{\mathrm{g}}^1$ holds and the request is accepted. As the responder moves closer, $\mathbf{x} \in \mathcal{P}_{\mathrm{y}}^1$ occurs, a conflict becomes possible, and the request is accepted with a suggestion: the requesting vehicle 2 shall clear the conflict zone by $T_1^{\max}$. Note that the value of $T_1^{\max}$ decreases as the responder approaches. When $T_1^{\max} < T_2^{\min}$, no feasible suggestion exist any more, leading to the rejection of request in the $\mathcal{P}_{\mathrm{r}}^1$ region. Observe from Fig. 5(c)-(d) that with higher approaching speed, the response transition from "accept" to "reject" occurs earlier. This demonstrates our framework's capability of providing preference-based response in negotiation.

Now we quantify the benefits of negotiation while considering status and intent sharing as a baseline. Using the experiment with 30 [mi/hr] target speed as an example, a zoomed-in view of the responder's conflict analysis is shown in Fig. 6(a). Under negotiation, there exists an 8.1 [s] opportunity window for the requesting vehicle 2 to pass first. During such window, $\mathbf{x} \in \mathcal{P}_{\mathrm{g}}^1 \cup \mathcal{P}_{\mathrm{y}}^1$ holds and the pass-first request is acceptable. Note that a larger pass-first opportunity window leads to better time efficiency of the vehicle 2 and improved traffic throughput of the intersection. Such window can thus be used to quantify the benefits of negotiation. If the vehicle 2 had not initiated a request, then it passes first when $\mathbf{x} \in \mathcal{P}_{\mathrm{g}}^2$ and yields when $\mathbf{x} \in \mathcal{P}_{\mathrm{y}}^2$ and $\mathcal{P}_{\mathrm{r}}^2$ [13]. The corresponding conflict analysis from vehicle 2's perspective is shown in Fig. 6(b); cf. Theorem 1. Noting that $\mathcal{P}_{\mathrm{g}}^1 \cup \mathcal{P}_{\mathrm{y}}^1 = \mathcal{P}_{\mathrm{g}}^2 \cup \mathcal{P}_{\mathrm{y}}^2$, negotiation provides additional pass-first opportunity for the region $\mathcal{P}_{\mathrm{y}}^2$ compared to intent sharing, as the latter only yields a pass-first window of 7.5 [s].

Our conflict analysis so far ignored potential time delays in negotiation. Indeed, negotiation delay in our experiments was small. The average CPU computation time of conflict analysis was measured to be 2.5 [ms], while the total communication time between a request being sent and a corresponding response being received averaged 32.4 [ms]. However, larger delays may exist in real traffic depending on communication conditions, and their effects on negotiation must be considered in conflict analysis. Although mathematically rigorous study is left for future work, here we evaluate the effects of response delay using the experimental data.

Consider a time gap τ between a request being received by the responder and the corresponding response being delivered to the requester. In our experimental scenario, the requester remains static during such response delay and only acts after receiving the response. With delay τ considered in

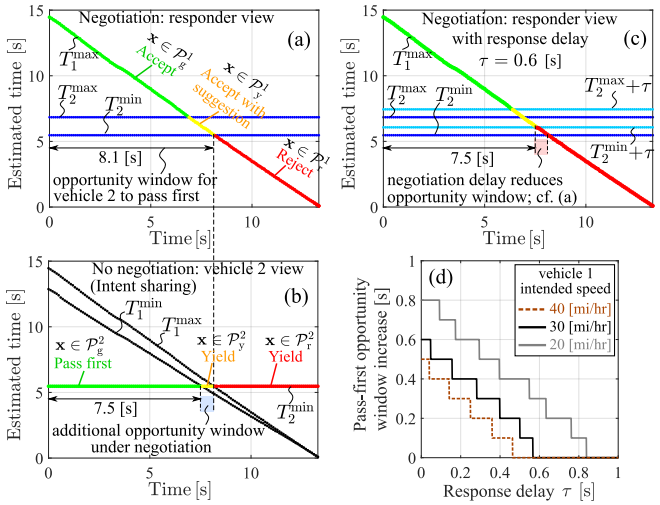

Fig. 6. Quantifying the benefits of negotiation using pass-first opportunity window of the turning vehicle 2. Using the data of 30 [mi/hr] responder approaching speed, conflict analysis is shown from the perspectives of (a) the responding vehicle 1; (b) the turning vehicle 2 under intent sharing; and (c) the responding vehicle 1 with response delay $\tau = 0.6$ [s]. (d) The increase of pass-first opportunity window (compared to intent sharing) as a function of response delay under different responder approaching speeds.

the responder's conflict analysis, the estimated minimum and maximum times of the requesting vehicle 2 exiting the conflict zone become $T_2^{\min} + \tau$ and $T_2^{\max} + \tau$, respectively. Meanwhile, the estimated maximum time $T_1^{\max}$ of the responder entering the conflict zone remains unchanged. This leads to the conflict analysis in Fig. 6(c), where under the response delay $\tau = 0.6$ [s], the pass-first opportunity window of vehicle 2 shrinks to 7.5 [s], which is the same as for the intent sharing case. Such τ represents the critical response delay, under which the advantage of negotiation over intent sharing vanishes.

Using intent sharing as a baseline, Fig. 6(d) quantifies the negotiation-enabled increase of pass-first opportunity window as a function of response delay for different approaching speeds of the responder. The benefit of negotiation diminishes as the delay increases, and higher speeds of the responder lead to smaller critical delays. This indicates that negotiation under higher speeds can be more vulnerable to communication delays. The discrete jumps in these plots are due to the fact that conflict analysis of the responder is performed only at the discrete times when request was received (every 0.1 [s]).

V. Conclusion

In this paper we constructed a framework for negotiation in cooperative maneuvering. Conflict analysis was used for feasible request initiation and response generation considering user-based behavior preferences. We implemented wireless negotiation messages using commercially available V2X communication devices, and validated the developed framework via experiments using real vehicles. Experimental results demonstrated that compared to receiving status and intent information only, negotiation can significantly benefit a vehicle's time efficiency by eliminating uncertainties in predicting surrounding vehicles' future behaviors, while ensuring safety. Such benefits, however, deteriorate under communication delays in negotiation. We quantified the benefits of negotiation and how these benefits degrade with time delays. Our future work includes comprehensive testing of intent-sharing and negotiation with automated vehicles, and extending the framework to more general traffic environments where non-connected road users exist.

Appendix I
Proof of Theorem 1

The definitions of $T_1^{\min}$ and $T_1^{\max}$ imply that $s_1(t) = s_1^{\text{in}}$ must hold for some $t = t_1 \in [T_1^{\min}, T_1^{\max}]$, $\forall u_1(t)$. Similarly, the definitions of $T_2^{\min}$ and $T_2^{\max}$ imply that $s_2(t) = s_2^{\text{out}}$ must hold for some $t = t_2 \in [T_2^{\min}, T_2^{\max}]$, $\forall u_2(t)$. Noticing that the functions $s_1(t)$ and $s_2(t)$ are non-decreasing along time t, the proposition P is equivalent to the condition $t_2 \leq t_1$. Using this fact, the relationships (10), (12), and (13) are obvious. These, together with the relationships $\mathbf{x} \in \mathcal{P}_{\text{y}}^1 \iff \mathbf{x} \notin \mathcal{P}_{\text{g}}^1 \wedge \mathbf{x} \notin \mathcal{P}_{\text{r}}^1$ and $\mathbf{x} \in \mathcal{P}_{\text{y}}^2 \iff \mathbf{x} \notin \mathcal{P}_{\text{g}}^2 \wedge \mathbf{x} \notin \mathcal{P}_{\text{r}}^2$ yield (11) and (14).

References

[1] L. Hobert, A. Festag, I. Llatser, L. Altomare, F. Visintainer, and A. Kovacs, "Enhancements of V2X communication in support of cooperative autonomous driving," *IEEE Communications Magazine*, vol. 53, no. 12, pp. 64–70, 2015.

[2] B. Häfner, V. Bajpai, J. Ott, and G. A. Schmitt, "A survey on cooperative architectures and maneuvers for connected and automated vehicles," *IEEE Communications Surveys & Tutorials*, vol. 24, no. 1, pp. 380–403, 2022.

[3] SAE J3216, "Taxonomy and Definitions for Terms Related to Cooperative Driving Automation for On-Road Motor Vehicles," SAE International, Tech. Rep., 2020.

[4] SAE J2735, "Dedicated Short Range Communications (DSRC) Message Set Dictionary Set," SAE International, Tech. Rep., 2016.

[5] S. Oh, Q. Chen, H. E. Tseng, G. Pandey, and G. Orosz, "Sharable clothoid-based continuous motion planning for connected automated vehicles," *arXiv preprint arXiv:2312.10880*, 2023.

[6] H. M. Wang, S. S. Avedisov, O. Altintas, and G. Orosz, "Experimental validation of intent sharing in cooperative maneuvering," in *IEEE Intelligent Vehicles Symposium (IV)*, 2023, pp. 1–6.

[7] SAE J3186, "Application Protocol and Requirements for Maneuver Sharing and Coordinating Service," SAE International, Tech. Rep., work in progress. Available: https://www.sae.org/standards/content/j3186/.

[8] *Intelligent Transport Systems (ITS); Vehicular Communications; Informative report for the Maneuver Coordination Service*, ETSI TR 103 578 Std., draft 0.0.7, Feb. 2022.

[9] I. Llatser, T. Michalke, M. Dolgov, F. Wildschütte, and H. Fuchs, "Cooperative automated driving use cases for 5G V2X communication," in *2nd IEEE 5G World Forum (5GWF)*, 2019, pp. 120–125.

[10] B. Lehmann, H.-J. Günther, and L. Wolf, "A generic approach towards maneuver coordination for automated vehicles," in *2018 21st International Conference on Intelligent Transportation Systems (ITSC)*. IEEE, 2018, pp. 3333–3339.

[11] D. Heß, R. Lattarulo, J. Pérez, T. Hesse, and F. Köster, "Negotiation of cooperative maneuvers for automated vehicles: Experimental results," in *2019 IEEE Intelligent Transportation Systems Conference (ITSC)*, 2019, pp. 1545–1551.

[12] D. Maksimovski and C. Facchi, "Negotiation patterns for V2X cooperative driving: How complex maneuver coordination can be?" in *IEEE 98th Vehicular Technology Conference (VTC2023-Fall)*, 2023, pp. 1–7.

[13] H. M. Wang, S. S. Avedisov, T. G. Molnár, A. H. Sakr, O. Altintas, and G. Orosz, "Conflict analysis for cooperative maneuvering with status and intent sharing via V2X communication," *IEEE Transactions on Intelligent Vehicles*, vol. 8, no. 2, pp. 1105–1118, 2023.

[14] *IEEE Standard for Wireless Access in Vehicular Environments (WAVE)–Networking Services*, IEEE Std., 1609.3-2020, Dec. 2020.